IIETA International Information and Engineering Technology Association
Advancing the World of Information and Engineering

Traitement du Signal
Vol. 43, No. 2, April, 2026, pp. 1023-1037
Journal homepage: http://iieta.org/journals/ts

Fractal-Based Functional Connectivity Analysis of Electroencephalography Signals for Alcohol Use Disorder Characterization

Maisarah Rafiq Faisal Rafiq[1], Norashikin Yahya[2*], Lok Hua Lee[2], Nasreen Badruddin[2], Ashvaany Egambaram[2], Danish M. Khan[3], Nidal S. Kamel[4], Mohammed J. Abdulaal[5]

[1] Instrumentation and Telecommunication Department, McDermott Asia Pacific Sdn Bhd, Kuala Lumpur 50470, Malaysia
[2] Centre for Intelligent Signal and Image Research (CISIR), Electrical and Electronic Engineering, Universiti Teknologi PETRONAS, Seri Iskandar 32610, Malaysia
[3] School of Computing and Artificial Intelligence, Sunway University, Bandar Sunway 47500, Malaysia
[4] College of Engineering and Computer Science, VinUniversity, Hanoi 100000, Vietnam
[5] Center of Excellence in Intelligent Engineering Systems (CEIES), Department of Electrical and Computer Engineering, Faculty of Engineering, King Abdulaziz University, Jeddah 21589, Saudi Arabia

Corresponding Author Email: norashikin_yahya@utp.edu.my

https://doi.org/10.18280/ts.430237

Received: 19 January 2026
Revised: 2 April 2026
Accepted: 16 April 2026
Available online: 30 April 2026

Keywords:
electroencephalography signal processing, fractal decomposition, functional connectivity, default mode network, Alcohol Use Disorder

ABSTRACT

Alcohol Use Disorder (AUD) is associated with alterations in large-scale brain networks that are not always captured by conventional symptom-based diagnostic frameworks. Electroencephalography (EEG), as a non-invasive and high-temporal-resolution modality, provides a valuable means for investigating such alterations through signal-based biomarkers. In this study, we investigate a signal-processing approach for AUD characterization by applying fractal decomposition to EEG-derived functional connectivity (FC). Resting-state EEG signals recorded from 30 AUD subjects and 30 healthy controls were analyzed by separating oscillatory and scale-free (fractal) components using fractal decomposition. Functional connectivity was then estimated among selected default mode network (DMN) channels, and correlation-based connectivity matrices were constructed for the original, fractal, and non-fractal signal components. The upper-triangular connectivity coefficients were aggregated to form compact feature representations that preserve network-level signal interactions. The discriminative capability of these features was evaluated using Optimizable Support Vector Machine (SVM) and Ensemble classifiers. The results show that connectivity features derived from decomposed signals achieve classification accuracies of up to 85.86%, with the original and non-fractal components providing comparable performance and the fractal component contributing complementary information. Comparative and ablation analyses further demonstrate how separating oscillatory and scale-free components influences the representation of connectivity patterns associated with AUD. These findings suggest that incorporating fractal decomposition into connectivity analysis provides additional insight into EEG signal structure and may support the development of more informative signal representations for neurological disorder assessment.

1. INTRODUCTION

Alcohol consumption is widespread globally, and excessive intake can result in significant neurological, cognitive, and behavioral impairments [1, 2]. Prolonged alcohol dependence, clinically categorized as Alcohol Use Disorder (AUD), has been associated with structural and functional alterations in the brain that adversely affect cognitive processing, motor coordination, memory, and emotional regulation [3-7]. According to the Diagnostic and Statistical Manual of Mental Disorders, Fifth Edition (DSM-5) [8], AUD diagnosis is primarily based on symptom clusters and behavioral assessments, which remain inherently subjective and vulnerable to reporting bias.

AUD has been consistently associated with disruptions in large-scale brain network organization, including altered functional connectivity (FC), impaired inter-regional communication, and reduced efficiency of information transfer [9-11]. In addition to these connectivity-level abnormalities, prior studies have reported that AUD is characterized by alterations in the intrinsic dynamics of electroencephalograph (EEG) signals, including reduced signal complexity and modified nonlinear behavior [12, 13].

From a signal processing perspective, EEG signals exhibit scale-free and self-similar characteristics, reflecting long-range temporal dependencies and broadband background activity that are not fully captured by conventional oscillatory or frequency-domain analyses. Fractal decomposition provides a principled framework for separating oscillatory and non-oscillatory components, thereby enabling the

characterization of both rhythmic activity and scale-invariant dynamics within the same signal representation. In the context of AUD, where both FC and signal complexity are affected, such decomposition facilitates a more comprehensive analysis of neural interactions by isolating components that may differentially reflect pathological alterations. Consequently, the use of fractal decomposition in this study is motivated by its ability to capture underlying scale-free properties of EEG signals that are directly relevant to AUD-related neural dysfunction.

Recent EEG-based studies have demonstrated that alterations in rhythmic activity and inter-regional coupling can serve as informative markers for neurological and neuropsychiatric conditions. In particular, FC analysis provides a principled framework for characterizing coordinated activity between spatially distributed brain regions, thereby enabling network-level interpretation of neural signals [14, 15]. Alterations in FC patterns have been consistently reported across a range of neurological and neuropsychiatric conditions, including depression, schizophrenia, epilepsy, stroke, and substance-related disorders, highlighting the diagnostic potential of connectivity-based signal representations [16-20].

In particular, FC analysis provides a framework for characterizing coordinated activity between spatially distributed brain regions, enabling network-level interpretation of neural signals. Variations in FC patterns have been reported in conditions such as depression, schizophrenia, stroke, and substance-related disorders, highlighting the diagnostic potential of connectivity-based signal representations [15, 18, 21-24].

1.1 Related work on Alcohol Use Disorder classification

Recent studies have increasingly highlighted the potential of FC derived from EEG signals as a promising feature for classifying various neuropsychiatric disorders, including AUD. For example, one study involving EEG data from 24 patients with Major Depressive Disorder (MDD) and 29 healthy controls applied intrinsic time-scale decomposition (ITD) and a graph-based adaptive least absolute shrinkage and selection operator (GA-LASSO) model to extract time–frequency characteristics of FC for classification [25]. Several classifiers were evaluated, including Support Vector Machine (SVM), k-Nearest Neighbour (kNN), Long Short-Term Memory (LSTM), and Convolutional Neural Network (CNN), with SVM achieving the highest accuracy of 97.43%.

Similarly, another study used FC features as input to a SelectKBest algorithm combined with a CNN to classify autism spectrum disorder (ASD) [26]. Resting-state EEG data from 189 subjects (97 with ASD and 92 healthy controls) were analyzed, achieving an accuracy of 81.08%. These findings emphasize the importance of FC in capturing brain activity and its effectiveness as a biological feature for neuropsychiatric disorder classification.

In 2022, a study employed a multilayer discrete wavelet transform (DWT) to decompose, denoise, and extract EEG features for AUD classification from 122 subjects [27]. As a time–frequency analysis model, DWT enables the identification of key signal characteristics across both domains. A hybrid deep learning model combining Convolutional Neural Networks (CNN) and Bidirectional Long Short-Term Memory (Bi-LSTM) networks (CNN–Bi-LSTM) was then applied, achieving an accuracy of 99.32%. In earlier work, AUD classification using EEG signals was also explored with effective connectivity (EC) as a biomarker rather than FC [28]. In particular, the study [28] used Partial Directed Coherence (PDC) as the EC feature extraction method, paired with a 3D-CNN classifier on data from 31 AUD patients and 31 healthy controls, yielding an accuracy of $87.85 \pm 4.64\%$. By employing frequency-domain analysis, the study highlighted the strength of causal interactions between brain regions within the default mode network (DMN) as a distinguishing feature between AUD patients and healthy controls (HC).

Recent studies have also explored fractal analysis of EEG signals as an effective analytical feature for machine learning and deep learning algorithms. In one such study [13], discriminative features were extracted from EEG signals of 10 healthy subjects and 10 AUD patients using the Davies–Bouldin (DB) criterion, which assesses the separability of feature clusters based on their distribution. The results of the DB analysis were subsequently fed into two classifiers—SVM and kNN—achieving accuracies of 98.77% and 98.5%, respectively, thereby demonstrating the effectiveness of fractal features as reliable indicators for AUD classification using EEG signals.

Another study applied Hurst exponent estimation and adaptive fractal analysis (AFA) of EEG signals to classify epileptic and non-epileptic patients [29]. Hurst exponent-based time-domain analysis was employed to examine the signal's scaling properties, while Adaptive decomposition analysis (ADA) was utilized for its robustness to noise. The study [29] used an extensive dataset of 11,500 samples with 178 features each. The fractal analysis output was then fed into a Support Vector Regression (SVR) model and a multilayer Gradient Boosting Decision Tree (GBDT), achieving a peak accuracy of 98.23%.

Wavelet-based fractal analysis of fMRI data has also emerged as a promising approach for diagnostic modeling [30]. Another study used fMRI signals to capture the fractal behavior of FC features for Alzheimer's disease classification [31]. This comparative study included two datasets: the first with 21 normal controls and 35 AD patients, and the second with 30 normal controls and 30 AD patients. Wavelet-based fractal analysis was conducted to decompose the fMRI signals into fractal and non-fractal components for feature extraction. In addition, Pearson correlation was employed as a baseline method for comparison. The resulting features were then used to train an SVM classifier for the classification task. A maximum accuracy of 90.3% was achieved using the non-fractal-based method, highlighting that non-fractal components are effective for representing spontaneous FC in characteristics neurological disorders.

Hadiyoso et al. [32] examined EEG signal complexity for early Alzheimer's Dementia detection using entropy and fractal features from resting-state EEG. Spectral entropy and fractal dimensions (Higuchi, Katz, and Sevcik) were extracted from 19-channel EEG recordings of 34 subjects (normal elderly and MCI). Using Linear Discriminant Analysis, the study found reduced EEG complexity in MCI subjects, particularly in frontal and occipital regions. The combined entropy–fractal feature set achieved 82.4% accuracy, 87.5% sensitivity, and 77.8% specificity, demonstrating the effectiveness of complexity-based features in capturing subtle neural changes while reducing sensitivity to low-frequency noise.

This work reinforces the relevance of complexity-driven

EEG signal analysis as a complementary methodology for neurodegenerative disorder assessment and motivates further exploration of fractal-informed signal features at higher representational levels, such as FC analysis.

Beyond conventional time–frequency analysis, EEG signals are known to exhibit scale-free and self-similar characteristics, often described using fractal models [30, 33]. Fractal analysis enables the separation of broadband, non-oscillatory background activity from narrowband oscillatory components, thereby offering a more comprehensive representation of neural signal structure. While fractal measures have previously been employed as standalone features for classification, their integration into connectivity-level signal analysis remains relatively underexplored.

Motivated by this gap, the present study proposes a fractal-based FC framework for EEG analysis in AUD. By applying fractal decomposition prior to connectivity estimation, the proposed approach isolates oscillatory and scale-free components and examines their respective contributions to network-level interactions within the DMN. This signal-centric methodology enables the extraction of biologically meaningful connectivity features that reflect long-range temporal dependencies and coordination patterns often obscured in conventional analyses.

Machine learning classifiers are employed in this study solely as quantitative evaluation tools to assess the discriminative capability of the extracted signal features. The main contribution of this work lies in the systematic application and evaluation of fractal decomposition within a FC framework for EEG analysis in AUD. Specifically, the study examines how separating oscillatory and scale-free components influences connectivity-based feature representations, and compares their respective contributions through an ablation-style analysis. By providing a structured comparison of original, fractal, and non-fractal connectivity features within the same analytical pipeline, this work offers additional insight into the role of scale-invariant dynamics in EEG-based connectivity analysis, rather than introducing a fundamentally new methodological approach.

1.2 Default mode network channels

The brain network associated with cognitive functioning is known as the DMN. According to Menon [34], the DMN is closely associated with cognitive functions, particularly retrospective processes such as episodic memory, social cognition, and semantic memory, which are sustained over time—making it a suitable framework for detecting neural irregularities during simulated tasks. Resting-state EEG signals, especially those originating from the DMN, exhibit intrinsic dynamics that not only reflect brain adaptability but also serve as predictors of cognitive performance [35, 36]. These patterns have been widely used to investigate the pathophysiology of psychological disorders such as post-traumatic stress disorder (PTSD), schizophrenia (SZ), and MDD [37, 38].

The DMN primarily comprises key brain regions such as the posterior cingulate cortex (PCC), medial prefrontal cortex (mPFC), and the precuneus, which maintains FC with the inferior parietal cortex (IPC) [34, 39], as illustrated in Figure 1. These regions collectively underpin the brain's baseline neural activity and are crucial for internally directed cognitive processes such as self-referential thinking and memory consolidation [39]. Rather than assessing isolation, the correlation of these regions was studied to provide insight into brain activity, known as FC [37]. To capture this connectivity, EEG channels located nearest to canonical DMN regions were identified and mapped to corresponding Brodmann areas [40]. Consequently, six EEG electrodes (Pz, Fz, F3, F4, P3, and P4) were exclusively selected, as they provide the most reliable representation of the DMN's functional architecture and are therefore most appropriate for feature extraction and detailed analysis [28], as summarized in Table 1. This electrode selection is further supported by prior EEG and neuroimaging studies that have established spatial correspondences between scalp-recorded signals and underlying DMN regions. Frontal electrodes such as Fz, F3, and F4 are commonly associated with activity in the medial prefrontal cortex (mPFC), a core hub of the DMN involved in self-referential and executive processes [7, 34]. Similarly, parietal electrodes including Pz, P3, and P4 have been linked to posterior DMN regions such as the precuneus and PCC, which play a central role in internally directed cognition and memory integration [36, 39]. EEG-fMRI studies have further demonstrated that FC patterns observed at these electrode sites reflect large-scale network interactions consistent with DMN organization [37]. Moreover, alterations in frontal–parietal connectivity involving these regions have been consistently reported in neuropsychiatric conditions, including AUD, reinforcing their relevance for capturing network-level dysfunction [28, 41].

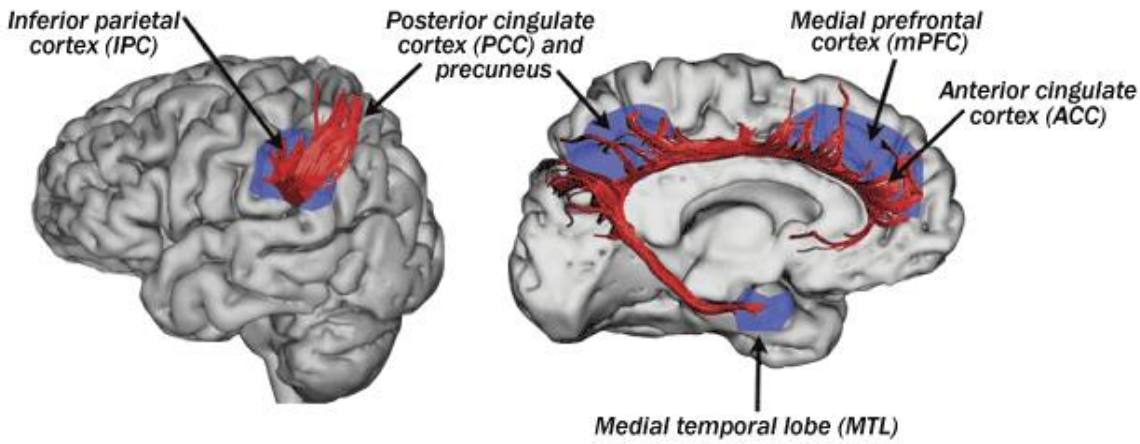

Figure 1. Lateral and medial view of the default mode network (DMN) of the left hemisphere (adapted and modified from [37])

Table 1. Electroencephalograph (EEG) electrode locations corresponding to default mode network (DMN) regions and associated Brodmann areas used for feature extraction. L and R denote the left and right hemispheres, respectively

DMN Region	Brodmann Area	Electrode
Precuneus	BA07	Pz
mPFC	BA08/09	Fz
mPFC	BA08/09L	F3
mPFC	BA08/09R	F4
IPC	BA39/40L	P3
IPC	BA39/40R	P4

2. METHODOLOGY

The proposed methodology consists of four main steps: EEG data pre-processing, extraction of FC characteristics through fractal decomposition, data splitting for machine learning (ML) classification, and performance evaluation using ML performance metrics, as outlined in Figure 2. All analyses were conducted using MATLAB R2024a with the MathWorks Statistics and Machine Learning Toolbox on an HP Pavilion workstation.

2.1 Electroencephalograph signals datasets and pre-processing

The EEG dataset used in this project was acquired from 30 AUD patients and 30 healthy subjects, with the sample distribution illustrated in Figure 3. Data collection for all AUD patients and 19 healthy subjects was ethically conducted at Universiti Malaya Medical Center (UMMC) and Bingkor Clinic in Kota Kinabalu, Sabah, Malaysia. The data for the remaining 11 healthy subjects were collected at Universiti Teknologi PETRONAS. This dataset was also used [28]. However, it is important to note that the relatively small sample size and the geographic concentration of participants within Malaysia may limit the representativeness of the dataset. These factors could affect the generalizability of the findings to broader populations with different demographic or cultural characteristics.

The AUD group had a mean age of 55.2 ± 12.8 years, while the HC group had a mean age of 48 ± 10.3 years; all participants were right-handed. Although the age ranges of the two groups overlap, the difference in mean age may introduce a potential confounding effect. Future work will address this limitation by employing age-matched cohorts and incorporating age as a covariate in the statistical analysis.

Subjects in the AUD group met DSM-5 diagnostic criteria for alcohol dependence or abuse. Participation required informed consent, and exclusion criteria included age below 18 years, dependence on substances other than alcohol, presence of medical or psychiatric conditions, allergy to diazepam, or refusal to provide consent.

EEG recordings were obtained over a 5-minute period under eyes-closed resting-state conditions, conducted in the morning within a soundproof room. During data acquisition, participants were instructed to remain relaxed and refrain from any limb movements. The raw EEG data underwent standardized preprocessing prior to feature extraction. All recordings were first downsampled to 256 Hz and converted to a consistent amplitude scale. The signals were then re-referenced to the Cz electrode to ensure uniformity across recording systems. A bandpass filter in the range of 0.1–70 Hz was applied to preserve relevant neural activity, followed by a 50 Hz notch filter to eliminate power line interference.

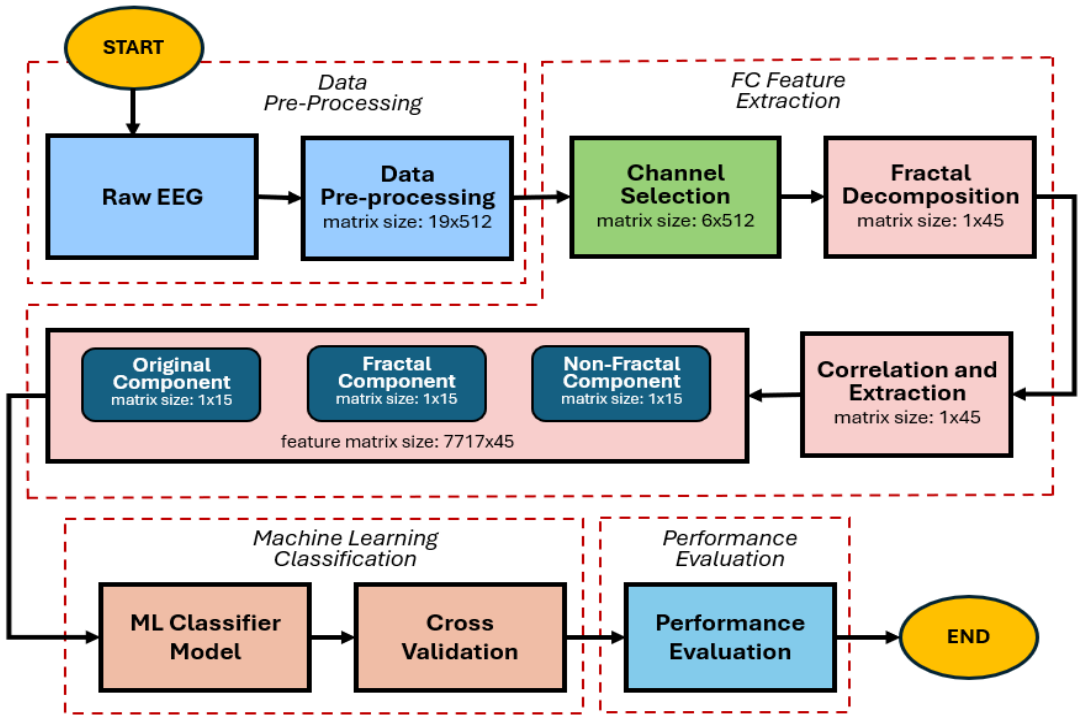

Figure 2. Overall workflow of the proposed machine learning framework for Alcohol Use Disorder (AUD) versus healthy controls (HC) classification using fractal-based functional connectivity (FC) features, including electroencephalograph (EEG) pre-processing, FC feature extraction via fractal decomposition, machine learning classification, and performance evaluation. The original 19-channel EEG recordings were reduced to 6 channels, and fractal decomposition was applied on 2-second EEG windows (512 samples per channel)

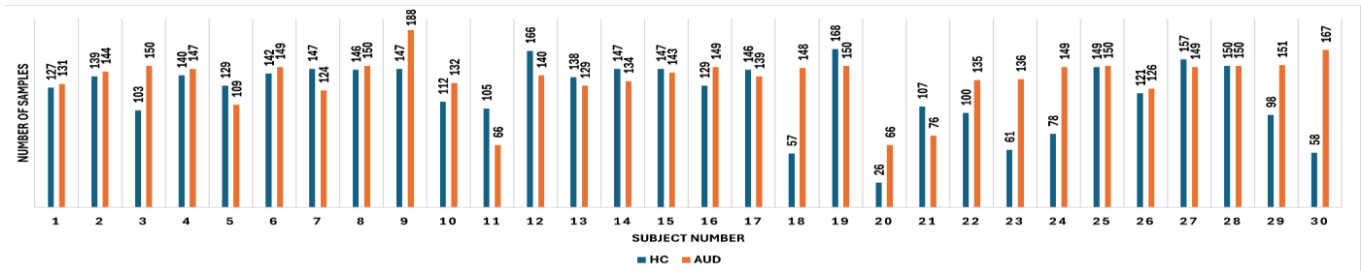

Figure 3. Distribution of samples for 30 Alcohol Use Disorder (AUD) and 30 healthy controls (HC) subjects

Artifact removal was performed using the Artifact Subspace Reconstruction (ASR) method implemented in the EEGLAB toolbox in MATLAB. The ASR algorithm was applied using its default parameter settings, where transient high-variance components were identified relative to a clean reference and automatically suppressed. As connectivity estimation is sensitive to preprocessing distortions, the cleaned signals were further inspected, and any remaining contaminated segments were excluded rather than corrected.

Following preprocessing, the EEG signals were segmented into multiple non-overlapping epochs of 2 seconds (512 samples per segment). This segment length was selected to ensure approximate signal stationarity [28], which is typically maintained for durations shorter than 4 seconds, while also providing a sufficient number of samples for reliable FC estimation and subsequent machine learning analysis.

2.2 Estimation of functional connectivity using fractal decomposition

Fractal decomposition of FC leverages the behavioral differences between oscillatory (non-fractal) and non-oscillatory (fractal) components of EEG signals to quantify brain activity correlations [42, 43]. This is achieved by redistributing oscillatory power while preserving fractal components through resampling and computing the geometric mean of the resampled signals. Given $P_f(f)$ as the fractal component of the power spectrum and $P_x(f)$ as the oscillatory component [42], the resampling process is mathematically expressed as follows:

$$S_h(f) = h^{2H} P_f(f) + P_x(fh) \tag{1}$$

where, h^{2H} represents the scaling of fractal components, with the Hurst exponent H quantifying long-range self-similarity. Thus, h^{2H} captures the self-similar nature of the fractal background, whereas $h \in \{1.10,1.90\}$ at step size of 0.05, denotes the resampling factor that shifts the oscillatory components. The resampling range (1.10–1.90) with a step size of 0.05 was adopted based on prior IRASA-based studies to ensure effective separation of oscillatory and fractal components, without performing additional parameter optimization in this work [44]. To estimate the fractal power spectrum, the geometric mean of resampled spectra is computed to suppress oscillatory peaks:

$$\widetilde{S_h}(f) = \sqrt{S_h(f) S_{1/h}(f)} \tag{2}$$

The final estimate of the fractal power spectrum is then obtained by taking the median across all resampling factors h:

$$\widehat{P_f}(f) = \text{median}_h \left(\widetilde{S_h}(f) \right) \tag{3}$$

Finally, let $P_y(f)$ be the original power spectrum. The oscillatory component $\widehat{P_x}(f)$ is then derived by subtracting the estimated fractal spectrum:

$$\widehat{P_x}(f) = P_y(f) - \widehat{P_f}(f) \tag{4}$$

The implementation of fractal decomposition of n-sample $\times$ c-channel EEG signals [42], is described in Algorithm I. To clarify, the input signal $x \in \mathbb{R}^{n \times c}$ is first segmented into 10 blocks, where the sample length of each block is equivalent to n $\times$ 0.90 and overlaps by 10% for each successive segment block, denoted as X_i, where i is the block index.

After segmenting the input signal, X_i is up- and down-sampled by a ratio ranging from 1.10 to 1.90 with a step size of 0.05. Fast Fourier Transform (FFT) is then applied to the originally segmented signal block as well as to the up- and down-sampled signals, using the estimated number of samples computed from the nearest power of two of the X_i sample size. All operations are performed channel-wise.

Following this, the geometric mean of the cross-spectrum signals—computed via element-wise multiplication of the post-FFT X_i conjugate with the up- and down-sampled signals, respectively—for all resampling ratios is obtained, and the median of all geometric means is computed.

Subsequently, the cross-spectrum of the post-FFT X_i is obtained through self-multiplication with its conjugate. Both the medians and the cross-spectrum of the post-FFT X_i are averaged to estimate the oscillatory component (i.e., the difference between the averaged cross-spectrum of post-FFT X_i and the medians) and the fractal component (i.e., the absolute value of the averaged medians). The code for Algorithm I is available online [45].

Ultimately, three 6 $\times$ 6 Pearson correlation matrices—corresponding to the original, fractal, and non-fractal components—are constructed to quantify the correlations among six DMN channels, as shown in Figure 4. These matrices capture the FC patterns in the EEG signals, effectively differentiating fractal, non-oscillatory activity from frequency-specific oscillatory dynamics.

To simplify the analysis, only the upper diagonal values of each correlation matrix are extracted into a 1 $\times$ 15 vector to avoid redundancy, as the upper and lower triangles of the matrix are mirrored and the diagonal values are always 1. The extracted components from all three matrices are aggregated into a 1 $\times$ 45 vector, representing the fractal-based FC features for a single 2-second sample (visualised in Figure 4). This process is repeated for all EEG samples, forming a complex coefficient matrix of size 7717 $\times$ 45 for the complete dataset of 60 subjects.

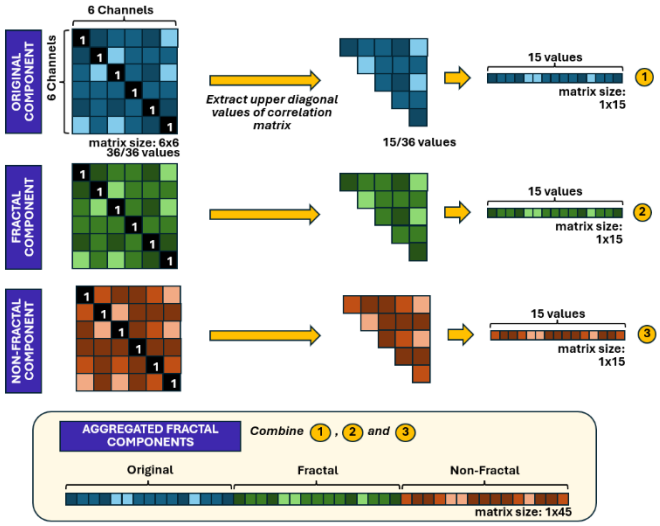

Figure 4. Extraction of upper diagonal correlation values and aggregation into a 1 × 45 functional connectivity (FC) feature vector

By extracting the upper diagonal values of the correlation matrices, these vectors can then be plotted to visualize the correlation patterns across samples. Figure 6 presents the fractal component pattern plots for one sample of an HC subject, where the value at index 16 represents the class label, indicated as 0 for HC. It can be observed that the fractal components consistently display smooth and high-magnitude trends, indicating stable and self-similar signal behavior typical of HC subjects. The combined overall pattern plot shows that the three components remain relatively close, with modest divergence and convergence points throughout the feature vector. Unlike the HC samples, the AUD samples exhibit more pronounced and dramatic fluctuations in their component patterns, as illustrated in Figure 6. This is especially evident in the erratic responses of the original component, as well as the significant variances between components. From the combined overall pattern plots, AUD subjects produce higher divergence and inconsistent responses across the indexes, resulting in less overlapping signals. These observations suggest less coordinated and more irregular behavior among the components in AUD subjects, which may be indicative of altered FC.

The implementation of fractal decomposition of n-sample × c-channel EEG signals, modified from [42], is provided in Algorithm 1. The MATLAB implementation is available online [45].

Ultimately, three 6 × 6 correlation matrices—corresponding to the original, fractal, and non-fractal components—are constructed to quantify the correlations among six DMN channels, as shown in Figure 5. These matrices capture the FC patterns in the EEG signals, effectively differentiating fractal, non-oscillatory activity from frequency-specific oscillatory dynamics.

Algorithm I: Fractal decomposition of $(n \times c)$ -EEG signal

Input variables

x: Input signal, $\mathbb{R}^{n \times c}$
n: Number of samples
c: Number of channels
h: Resampling values/rates

Initialize variables

$s_1 \leftarrow 1$
$h \leftarrow 1.1{:}\,0.05{:}\,1.9$

IRASA implementation

$x \leftarrow$ Load in input signal
$n_s \leftarrow n * 0.9$ (To segment x into 10 blocks)
$s \leftarrow$ Estimate the sample indexes for each segmented block with segment length, n_s, 10% overlap
for $i = 1$ to $length(s)$ **do**
  $X_i \leftarrow x_{s_i:s_{i+1}}$ of all channels
  for $j = 1$ to $length(h)$ **do**
    $p \leftarrow$ Next higher power of two of X_i samples
    $N \leftarrow 2^{p^2}$, estimated number of samples for Fast Fourier Transform (FFT)
    $x_u, x_d \leftarrow$ Up- and down-sample X_i using spline and $h(j)$
    $X_{FFT(X_i)}, X_{FFT(x_u)}, X_{FFT(x_d)} \leftarrow$ FFT X_i, x_u, x_d with N
    Find the geometric mean of element wise cross spectrum of $conj\left(X_{FFT(X_i)}\right)$ and $X_{FFT(x_u)}$, $X_{FFT(x_d)}$
    $y_i \leftarrow$ Compute the median of geometric mean of all resampled signal
    $z_i \leftarrow$ Compute the cross spectrum of $X_{FFT(X_i)}$
Compute the mean of all segment outputs y and z
Obtain the oscillatory $z - y$ and fractal components $abs(y)$

To simplify the analysis, only the upper triangular values of each correlation matrix are extracted into a 1 × 15 vector to avoid redundancy, since the upper and lower triangles are mirrored and the diagonal values are always equal to 1. The extracted components from all three matrices are then aggregated into a 1 × 45 vector, representing the fractal-based FC features for a single 2-second sample (visualised in Figure 4). This process is repeated for all EEG samples, resulting in a coefficient matrix of size 7717 × 45 for the complete dataset of 60 subjects.

By extracting the upper triangular values of the correlation matrices, the resulting vectors can be plotted to visualize correlation patterns across samples. Figure 6 presents the fractal component pattern plots for one sample from an HC subject, where the value at index 16 represents the class label (0 for HC). The fractal components consistently display smooth, high-magnitude trends, indicating stable and self-similar signal behavior typical of HC subjects. The combined overall pattern plot shows that the three components relatively close, with only modest points of divergence and convergence across the feature vector.

In contrast, AUD samples exhibit more pronounced and dramatic fluctuations in their component patterns, as illustrated in Figure 6. This is particularly evident in the erratic responses of the original component, as well as the large variances observed between components. In the combined overall pattern plots, AUD subjects demonstrate greater divergence and inconsistent responses across indices, resulting in reduced overlap among signals. These observations suggest less coordinated and more irregular behavior of the components in AUD subjects, which may reflect altered FC.

2.3 Machine learning classification of Alcohol Use Disorder vs. healthy controls

A comparative study was conducted using two machine

learning models: Optimizable SVM and Ensemble Learning. These models were employed as evaluation tools rather than representing the primary contribution of the study, with their selection motivated by their robustness in small-sample, high-dimensional settings.

After appending a label column, the coefficient matrix had a size of 7717 × 46 and served as the input for both classifiers. The models were trained and tested using a 90%–10% split to optimize classification performance. To ensure robustness and mitigate the limitations of a single train–test split, all performance results reported in Table 3 and Table 5 were obtained using stratified 10-fold cross-validation, repeated over 100 independent trials, with mean and standard deviation reported accordingly. This approach provides a more reliable estimate of model performance and reduces variance associated with small test sets.

		Original Component						Fractal Component						Non-Fractal Component					
		Channel						Channel						Channel					
		2	4	9	11	13	19	2	4	9	11	13	19	2	4	9	11	13	19
AUD	2	1	0.606	0.742	0.8171	0.8125	0.7262	1	0.8113	0.8822	0.7665	0.8569	0.8705	1	0.3431	0.7638	0.6231	0.645	0.5791
	4	0.606	1	0.6093	0.6338	0.7201	0.6185	0.8113	1	0.8182	0.82	0.8857	0.8675	0.3431	1	0.4363	0.3873	0.5012	0.3401
	9	0.742	0.6093	1	0.7156	0.7233	0.9123	0.8822	0.8182	1	0.6441	0.8257	0.9068	0.7638	0.4363	1	0.7166	0.6067	0.7536
	11	0.8171	0.6338	0.7156	1	0.921	0.803	0.7665	0.82	0.6441	1	0.8756	0.8106	0.6231	0.3873	0.7166	1	0.8163	0.7097
	13	0.8125	0.7201	0.7233	0.921	1	0.81	0.8569	0.8857	0.8257	0.8756	1	0.9543	0.645	0.5012	0.6067	0.8163	1	0.599
	19	0.7262	0.6185	0.9123	0.803	0.81	1	0.8705	0.8675	0.9068	0.8106	0.9543	1	0.5791	0.3401	0.7536	0.7097	0.599	1
HC	2	1	0.1075	0.5811	0.5873	0.0358	0.0666	1	0.5812	0.6671	0.7356	0.2497	0.4706	1	0.0978	0.5527	0.7562	0.0309	0.0495
	4	0.1075	1	0.1563	0.0517	0.9772	0.9907	0.5812	1	0.4448	0.4487	0.8117	0.9244	0.0978	1	0.1098	0.0669	0.9738	0.9894
	9	0.5811	0.1563	1	0.7861	0.1474	0.1436	0.6671	0.4448	1	0.8897	0.3854	0.4127	0.5527	0.1098	1	0.8018	0.0859	0.0886
	11	0.5873	0.0517	0.7861	1	0.0235	0.0276	0.7356	0.4487	0.8897	1	0.3011	0.401	0.7562	0.0669	0.8018	1	0.0245	0.0366
	13	0.0358	0.9772	0.1474	0.0235	1	0.9956	0.2497	0.8117	0.3854	0.3011	1	0.8436	0.0309	0.9738	0.0859	0.0245	1	0.9944
	19	0.0666	0.9907	0.1436	0.0276	0.9956	1	0.4706	0.9244	0.4127	0.401	0.8436	1	0.0495	0.9894	0.0886	0.0366	0.9944	1

Figure 5. Sample of 6 × 6 correlation matrix of six default mode network (DMN) channels (channel 2, 4, 9, 11, 13 and 19) for fractal, non-fractal and original signal components, shown for Alcohol Use Disorder (AUD) (top row) and HC (bottom row)

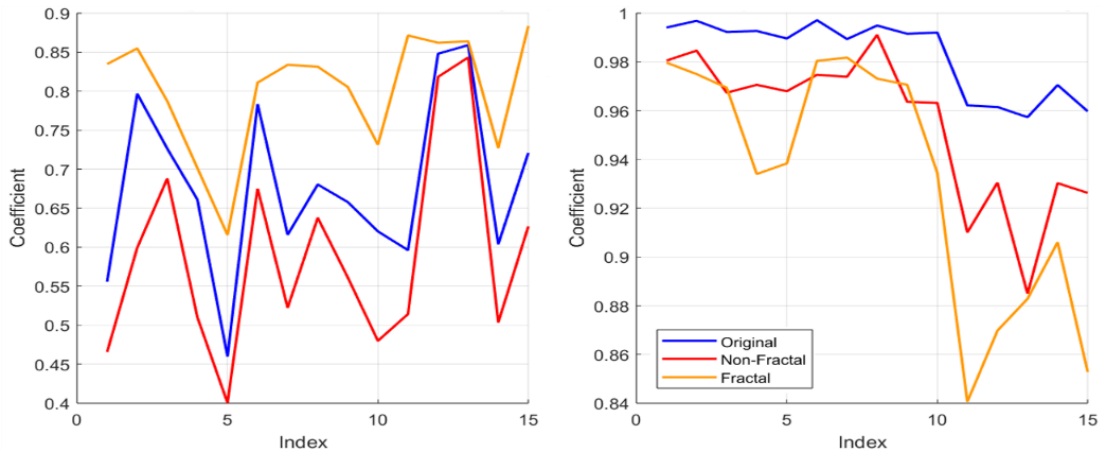

Figure 6. Visualization of functional connectivity (FC) patterns for fractal, non-fractal and original signal components from a 2-second segment, shown for Alcohol Use Disorder (AUD) (right) and healthy controls (HC) (left)

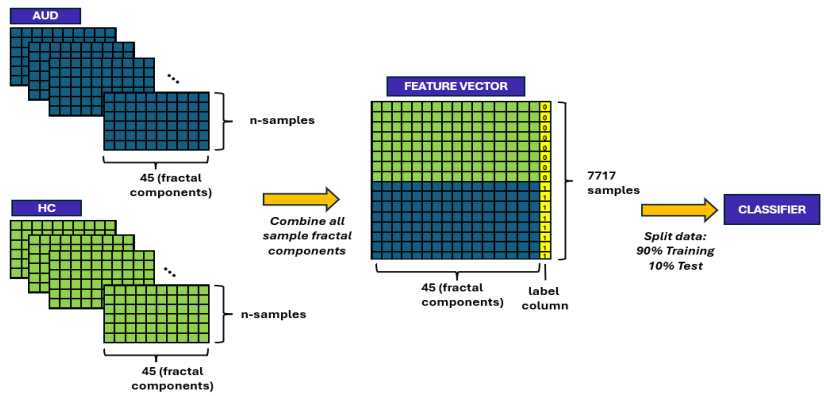

Figure 7. Workflow for training and testing a machine learning classifier using functional connectivity (FC) features. Each sample includes 45 features (15 original, 15 fractal, and 15 non-fractal components) extracted from Alcohol Use Disorder (AUD) and healthy controls (HC) groups. The 7717-sample dataset is labeled and split into 90% training and 10% testing sets for classifier evaluation

Performance was assessed using confusion matrices, statistical metrics (accuracy, sensitivity, specificity, and precision), and Area Under the Curve (AUC) scores. All operations were carried out using the Classification Learner App in MATLAB R2024b. The overall classification workflow is illustrated in Figure 7.

2.4 Model evaluation metrics

The classification results were statistically analyzed to evaluate the ability of the algorithm to distinguish AUD from healthy subjects. The following performance measures were derived from the confusion matrices:

$$Sensitivity = \frac{TP}{TP + FN} \tag{5}$$

$$Specificity = \frac{TN}{TN + FP} \tag{6}$$

$$Accuracy = \frac{TP + TN}{TP + TN + FP + FN} \tag{7}$$

$$Precision = \frac{TP}{TP + FP} \tag{8}$$

where, TP denotes True Positives, TN True Negatives, FP False Positives, and FN False Negatives. For this classification, AUD was defined as the positive class, while HC was considered the negative class. The Receiver Operating Characteristic (ROC) curve was also employed to evaluate the reliability of the model's binary classification by plotting the True Positive Rate (TPR) against the False Positive Rate (FPR). The Area Under the ROC Curve (AUC) serves as an indicator of how well the model discriminates between the two classes. Collectively, these measures provide insight into the model's reliability and its practical suitability for deployment.

3. RESULT AND DISCUSSION

The proposed method is evaluated across three dimensions: (i) feature-based analysis, which assesses the discriminative power of individual components—original, fractal, and non-fractal—using their respective feature vectors; (ii) sample-based testing, which measures overall classification performance using randomized training and testing splits; and (iii) subject-based testing, which examines subject dependency by reserving specific individuals exclusively for testing. All classifications are performed using two selected classifiers; Optimizable SVM and Ensemble Learning.

3.1 Linear and log-log scale power spectra analysis of original, fractal, and non-fractal connectivity

Power spectral density (PSD) analysis reveals how signal power is distributed across frequencies, capturing both rhythmic oscillations and background activity. The linear scale enables direct comparison of absolute power, making dominant rhythms and amplitudes more visible, while the log–log scale highlights scaling relationships and separates fractal background activity from oscillatory peaks. Using both views provides a fuller understanding of spectral patterns and the effectiveness of fractal decomposition in distinguishing neural components between AUD and HC subjects. Figure 8 shows the power spectra of a 2-second EEG segment for an AUD subject (top) and an HC subject (bottom) after fractal decomposition, in linear scale and log–log scale.

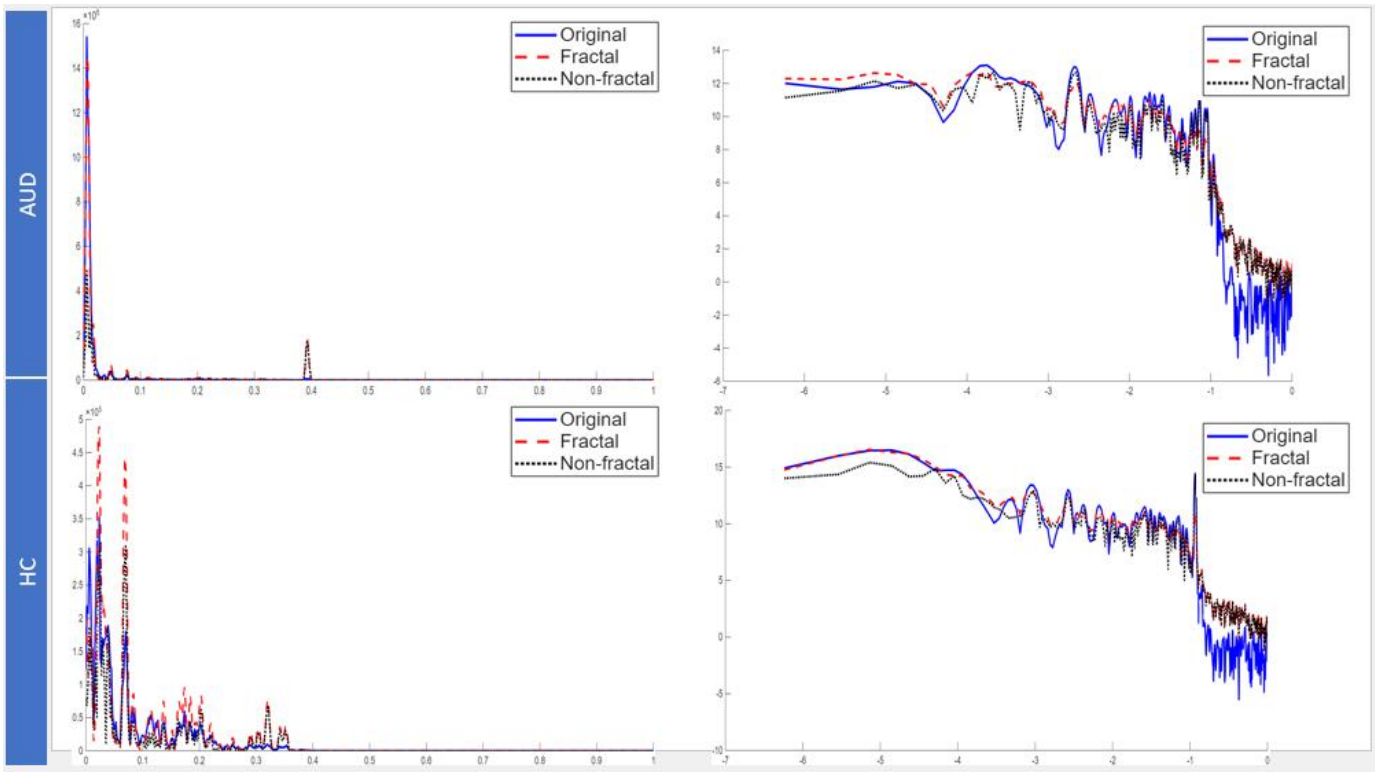

Figure 8. Power spectra in linear (left) and log-log (right) scale for fractal decomposition of a 2-second EEG segment from Alcohol Use Disorder (AUD) (top) and healthy controls (HC) (bottom). Each subplot compares the original, fractal, and non-fractal components, highlighting spectral differences between the AUD and HC

For the linear scale in Figure 8, the AUD subject exhibits a much higher low-frequency amplitude (16×10^6) with a large peak near 0 Hz, while the HC subject shows a lower amplitude (5×10^5) but a broader distribution of power between 0 and 0.4 Hz. Smaller peaks appear near 0.4 Hz in AUD and 0.1–0.2 Hz in HC, suggesting specific oscillatory components beyond the primary slow-wave peak. These patterns indicate reduced variety in rhythmic activity and stronger fractal background power in AUD, whereas HC displays more varied rhythms, which may be consistent with healthier and more active neural dynamics [42]. In AUD, the original component closely follows the fractal curve across 0–0.4 Hz, masking much of the non-fractal contribution. In contrast, the original component of the HC subject shows a clearer mix of both fractal and non-fractal patterns, with more distinct oscillatory peaks.

For the log–log scale in Figure 8, the AUD subject's spectrum shows irregular deviations from the expected smooth slope, including a marked drop in power near the frequency corresponding to −1 on the log scale. Such irregularities may reflect unstable oscillatory activity or increased noise influence. In contrast, the HC subject displays a more stable slope with well-defined oscillatory peaks, indicating more consistent rhythmic activity across frequencies. Moreover, the relationship between components shifts across frequencies. At low frequencies (around −6 to −2 on the log scale), the original component closely follows the fractal curve, indicating that fractal, non-oscillatory background activity dominates this range. However, from approximately −1 onwards, the fractal and non-fractal components align more closely with each other than with the original. This convergence reflects the reduced influence of the fractal background at higher frequencies, where the decomposition outputs share similar scaling behaviour. This characteristic is consistent with that observed in the linear plot.

3.2 P-value analysis of original, fractal, and non-fractal connectivity

To evaluate the discriminative capability of effective connectivity features between the Healthy Control (HC) and AUD groups, a statistical significance analysis was conducted using one-way ANOVA in MATLAB. A total of 45 connectivity features were extracted from pairwise interactions among six EEG channels within the DMN, comprising 15 original, 15 fractal, and 15 non-fractal features. The statistically significant connections with zero or near-zero p-values are summarized in Table 2. Following Benjamini–Hochberg FDR correction ($q = 0.05$), all previously identified significant connections (including those with near-zero p-values of 10^{-7} and 10^{-6}) remained significant after FDR correction, indicating that the findings are not due to multiple-comparison effects.

For both the original and fractal representations, the same eight connectivity links exhibited p-values equal to zero, indicating highly significant group-wise differences. These links primarily involve frontal–parietal and inter-frontal interactions, suggesting consistent alterations in long-range and frontal connectivity in the AUD group. Such disruptions are consistent with impaired frontoparietal executive networks reported in AUD, which underlie deficits in cognitive control and decision-making [28, 46]. In the non-fractal representation, six of these eight connections also retained zero p-values, while the remaining two links (Pz↔F3 and Pz↔F4) showed slightly higher but still highly significant p-values (10^{-7} and 10^{-6}, respectively). This indicates a minor reduction in statistical sensitivity for these specific connections when isolating the non-fractal component. Alterations involving frontal and parietal DMN nodes further align with evidence of DMN dysregulation in AUD, which has been linked to impairments in attention, memory, and executive function [47, 48].

These findings are in agreement with the power spectral analysis presented in Section 3.1. The original and non-fractal components preserved clearer oscillatory characteristics, which are known to be closely associated with neural communication and information transfer. In contrast, the fractal component predominantly captured broadband background activity, resulting in comparatively weaker discriminative capability despite the presence of statistically significant links. Moreover, the pronounced low-frequency dominance observed in the AUD group spectra further supports the observed *p*-value patterns, reinforcing the role of altered frontal–parietal connectivity in AUD-related neural dysfunction. Collectively, these results indicate that disrupted frontoparietal and DMN connectivity reflects impaired executive control and network-level dysregulation, key neurobiological mechanisms underlying AUD [28, 49].

Table 2. Comparison of effective connectivity measures between Healthy Control (HC) and Alcohol Use Disorder (AUD) Groups having zero p-value

Type	Link	p-Value	Mean HC	Mean AUD	STD
original	Pz↔Fz	0	0.55	0.44	0.25
original	Pz↔F3	0	0.79	0.84	0.19
original	Fz↔F3	0	0.58	0.43	0.27
original	Pz↔F4	0	0.78	0.82	0.19
original	Fz↔F4	0	0.51	0.42	0.26
original	F3↔F4	0	0.78	0.85	0.2
original	Fz↔P3	0	0.69	0.62	0.27
original	P3↔P4	0	0.81	0.87	0.18
fractal	Pz↔Fz	0	0.52	0.41	0.25
fractal	Pz↔F3	0	0.77	0.82	0.19
fractal	Fz↔F3	0	0.55	0.41	0.27
fractal	Pz↔F4	0	0.76	0.81	0.19
fractal	Fz↔F4	0	0.49	0.39	0.27
fractal	F3↔F4	0	0.75	0.83	0.19
fractal	Fz↔P3	0	0.65	0.59	0.28
fractal	P3↔P4	0	0.79	0.85	0.19
non-fractal	Pz↔Fz	0	0.7	0.63	0.17
non-fractal	Fz↔F3	0	0.72	0.62	0.18
non-fractal	Fz↔F4	0	0.67	0.6	0.19
non-fractal	F3↔F4	0	0.83	0.86	0.13
non-fractal	Fz↔P3	0	0.78	0.74	0.17
non-fractal	P3↔P4	0	0.84	0.88	0.12
non-fractal	Pz↔F3	1×10^{-7}	0.84	0.85	0.13
non-fractal	Pz↔F4	2.4×10^{-6}	0.81	0.83	0.13

3.3 Comparative analysis of original, fractal, and non-fractal connectivity in Alcohol Use Disorder vs. healthy controls classification

The feature sets for the non-fractal, fractal, and original FC were divided into feature vectors of equal dimension (7717×15) and evaluated over 100 iterations. The results are presented in Table 3 and Table 4. In terms of classification accuracy, the original and non-fractal features exhibited comparable performance across both models, with the original feature set achieving the highest overall accuracy of 78.32% for the optimizable SVM and 80.23% for the Ensemble model.

These values represent an advantage of 0.8% and 0.7%, respectively, over the non-fractal features, further supporting the role of fractal decomposition by showing how separating components influences discriminative power, suggesting that the original feature set retains more discriminative information relevant to distinguishing AUD from HC subjects. Furthermore, the original feature set yielded superior specificity (87.05%) and precision (82.02%) with the Ensemble model, indicating stronger discriminative capability, particularly in minimizing false positives.

However, this gain in accuracy and specificity came at the expense of sensitivity, where both models showed reduced performance—70.78% for the SVM and 74.48% for the Ensemble—indicating a higher likelihood of false negatives in AUD detection. In contrast, the non-fractal feature set offered a more balanced trade-off, improving sensitivity (75.65% for the Ensemble) while maintaining competitive accuracy (79.53%) and stability across other metrics. Fractal features alone yielded the lowest sensitivity (68.54% for SVM and 73.10% for the Ensemble), although they maintained reasonable specificity and precision, which suggests that fractal components contribute complementary information rather than acting as a standalone discriminative feature set.

Table 3. Mean classification accuracy (in %) with standard deviation for original, fractal, and nonfractal functional connectivity (FC) features, evaluated using Optimizable Support Vector Machine (SVM) and Ensemble classifiers

Classifier	Original	Fractal	Non-Fractal
Optimisable Support Vector Machine	78.32 ± 0.0093	76.81 ± 0.0093	77.52 ± 0.0108
Ensemble	80.23 ± 0.0103	78.91 ± 0.0101	79.53 ± 0.0089

Table 4. Sensitivity, specificity, accuracy, and precision (in %)—for original, fractal, and non-fractal functional connectivity (FC) features using Optimizable Support Vector Machine (SVM) and Ensemble classifiers

	Original		Fractal		Non-Fractal	
Evaluation Metrics	Opt SVM	Ens.	Opt SVM	Ens.	Opt SVM	Ens.
Sensitivity	70.8	74.5	68.5	73.1	71.00	75.7
Specificity	85.1	85.4	84.2	84.1	83.3	83
Precision	80.9	82	79.5	80.5	79.1	79.8
Accuracy	78.3	80.2	76.8	78.9	77.5	79.5

Ultimately, while the original feature set produces higher accuracy, specificity, and precision values, it does so at the expense of sensitivity, leading to greater performance variability. Conversely, the non-fractal feature set offers a better balance across all performance metrics, maintaining lower variability while achieving comparable accuracy to the original feature classifications, thereby reinforcing the value of the ablation framework in revealing the distinct and complementary roles of fractal and non-fractal components.

From a clinical perspective, the observed trade-off between sensitivity and specificity has important implications for the practical utility of the proposed approach. Sensitivity reflects the ability to correctly identify AUD subjects, which is critical for early detection and timely intervention, as missed cases (false negatives) may delay treatment and worsen clinical outcomes. In contrast, specificity represents the ability to correctly identify healthy individuals, thereby reducing false positives and minimizing unnecessary psychological burden or clinical follow-up. In this study, the original feature set achieved higher specificity and precision but at the cost of reduced sensitivity, indicating a tendency toward conservative classification that favors minimizing false positives. Conversely, the non-fractal feature set provided improved sensitivity with slightly lower specificity, suggesting a more balanced detection capability. In real-world clinical screening scenarios, a higher sensitivity is often preferred to ensure that individuals with AUD are not overlooked, even if it leads to a moderate increase in false positives. However, for confirmatory diagnostic settings, higher specificity may be more desirable to avoid misclassification of healthy individuals. Therefore, the choice of feature representation and classification strategy should be guided by the intended clinical application, with the non-fractal features offering a more balanced trade-off and the original features favoring specificity-driven decision-making.

3.4 Sample-based evaluation of Alcohol Use Disorder vs. healthy controls classification using fractal-based functional connectivity

Table 5 presents the sample-based evaluation results for AUD vs. HC classification using fractal-based FC features. Overall, the Ensemble model demonstrates superior performance across most evaluation metrics, achieving the highest average accuracy (85.86%) compared to the Optimizable SVM (83.94%). This advantage extends to precision (87.88% vs. 85.98%) and sensitivity (81.26% vs. 78.96%), indicating the Ensemble's stronger ability to capture true positives. The higher AUC score of 0.904, relative to 0.8345 for the SVM, further underscores its superior discriminative capacity and adaptability to complex, high-dimensional EEG features.

The Ensemble's advantage can be attributed to its integration of multiple classifiers, which provides a more comprehensive interpretation of the fractal-based connectivity patterns. In contrast, the Optimizable SVM, while effective, relies on a single decision boundary, which may limit its ability to generalize across the variability inherent in EEG-derived connectivity features.

Table 5. Sensitivity, specificity, accuracy, precision (in %) and AUC of fractal-based functional connectivity (FC) classification using Optimizable Support Vector Machine (SVM) and Ensemble classifiers

Evaluation Metrics	Optimizable Support Vector Machine	Ensemble
Accuracy	83.94 ± 0.055	85.86 ± 0.472
Sensitivity	78.96 ± 0.0069	81.26 ± 0.0096
Specificity	88.45 ± 0.0049	89.98 ± 0.0066
Precision	85.95 ± 0.0041	87.88 ± 0.0068
AUC	0.89926 ± 0.0005	0.9335 ± 0.0019

Notably, the SVM shows a relative strength in specificity, achieving 88.45%, only slightly lower than the Ensemble's 89.98%. This reflects the SVM's conservative bias in classifying HC subjects, thereby reducing the likelihood of false positives. Such a property can be valuable in clinical settings, where minimizing the misdiagnosis of healthy

individuals is important. Ultimately, while both models exhibit distinct strengths, the Ensemble model performs slightly better than the Optimizable SVM, indicating enhanced adaptability to the complexity and high dimensionality of EEG data and providing a higher level of confidence in AUD patient diagnosis.

3.5 Subject-based evaluation of Alcohol Use Disorder vs. healthy controls classification using fractal-based functional connectivity

Resting-state FC features derived from EEG signals effectively capture subject-specific neural patterns associated with AUD and HC, supporting their utility in subject-level classification and evaluation [28, 50]. The dataset was divided and tested under this paradigm, with classification accuracy ranging from 30.3% to 100% for the Optimizable SVM model and from 28.30% to 100% for the Ensemble model, as shown in Table 6. Taking 70% as the baseline accuracy, the results indicate instances of misclassification and inconsistency across different subjects. The Optimizable SVM misclassified three HC subjects (20% HC misclassification rate) and one AUD subject (6.7% AUD misclassification rate), whereas the Ensemble model misclassified only two HC subjects (13.3% HC misclassification rate) and correctly classified all AUD cases (0% AUD misclassification rate).

Despite slightly higher variance in a few HC predictions, the Ensemble model consistently outperforms or matches the SVM, with its perfect AUD classification further highlighting its robustness. These findings suggest that although both models are influenced by inter-subject variability, the Ensemble model offers superior generalization and greater diagnostic reliability, particularly in AUD detection.

Analysis of the extended confusion matrix in Figure 9 reveals that although both models demonstrate stronger performance in classifying AUD subjects than HC subjects, the Ensemble model consistently outperforms the Optimizable SVM across key metrics. Specifically, it achieves higher AUD classification accuracy (93.89% vs. 91.96%) and better HC classification precision (83.15% vs. 81.12%).

This consistent advantage suggests that the Ensemble model employs a more flexible decision boundary, better capturing interclass variability, particularly within the more heterogeneous HC group. It also demonstrates higher specificity (94.53% vs. 92.85%), reducing false positives—an essential consideration in clinical settings to avoid mislabelling healthy individuals.

Further, the Ensemble model demonstrates higher precision (81.46%) compared to the SVM (79.10%), along with lower false positive (5.47% vs. 7.15%) and false negative rates (6.11% vs. 8.04%). Notably, the reduction in false negatives is clinically significant, as misclassifying AUD subjects as healthy could delay timely diagnosis and treatment. Although the improvements of approximately 2% may appear modest, they contribute to a higher overall accuracy (87.89% vs. 85.87%), highlighting the Ensemble model's superior reliability and robustness for AUD diagnosis.

Table 6. Classification performance of 15 healthy controls (test subjects 1 to 15) and 15 Alcohol Use Disorder (AUD) (test subjects 16 to 30)

			Optimizable SVM		Ensemble	
Subject No.	**Ground Truth**	**No. of Samples**	**Accuracy (%)**	**Result**	**Accuracy (%)**	**Result**
1	HC	131	78.63	HC	84.73	HC
2	HC	144	84.72	HC	88.89	HC
3	HC	150	86.67	HC	90.67	HC
4	HC	147	100	HC	100	HC
5	HC	109	66.06	AUD	79.82	HC
6	HC	149	67.79	AUD	60.4	AUD
7	HC	124	84.68	HC	71.11	HC
8	HC	150	86.67	HC	80	HC
9	HC	188	77.13	HC	84.57	HC
10	HC	132	30.3	AUD	28.3	AUD
11	HC	66	84.85	HC	100	HC
12	HC	140	99.29	HC	100	HC
13	HC	129	100	HC	100	HC
14	HC	134	94.03	HC	95.52	HC
15	HC	143	91.61	HC	88.11	HC
16	AUD	129	92.25	AUD	86.05	AUD
17	AUD	146	99.32	AUD	99.32	AUD
18	AUD	57	87.72	AUD	82.46	AUD
19	AUD	168	98.81	AUD	100	AUD
20	AUD	26	92.31	AUD	84.62	AUD
21	AUD	107	98.13	AUD	100	AUD
22	AUD	100	98	AUD	98	AUD
23	AUD	61	96.72	AUD	93.44	AUD
24	AUD	78	97.44	AUD	97.44	AUD
25	AUD	149	83.89	AUD	79.19	AUD
26	AUD	121	97.52	AUD	97.52	AUD
27	AUD	157	97.45	AUD	98.09	AUD
28	AUD	150	56.67	HC	88.67	AUD
29	AUD	98	96.94	AUD	97.96	AUD
30	AUD	58	100	AUD	98.28	AUD

Table 7. Comparison of proposed technique with related works

Ref.	Disease	Signal Type	Connectivity Type	HC	AUD	Classifier	Accuracy (%)
[9]	Alcohol Use Disorder	EEG	Functional Connectivity	30	30	Random Forest	80.0
[32]	Alzheimer's Disease	fMRI	Fractal	30	30	SVM	83.3
-	Alcohol Use Disorder	EEG	Fractal	30	30	Ensemble	85.86
	Alcohol Use Disorder	EEG	Fractal	30	30	Optimizable SVM	83.94

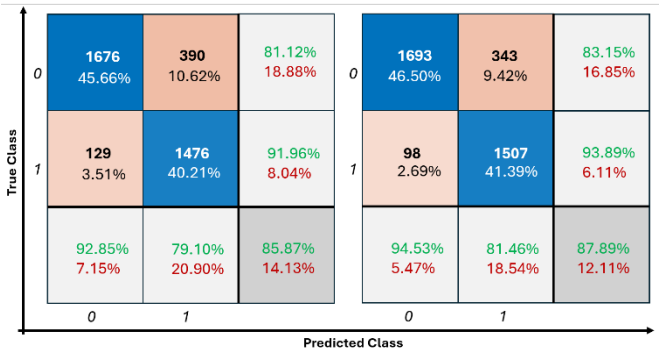

Figure 9. Extended confusion matrices for AUD classification using fractal-based functional connectivity (FC) with Optimizable SVM (left) and Ensemble (right). HC and AUD are encoded as 0 and 1, respectively; the vertical axis denotes the true class and the horizontal axis denotes the predicted class

Generally, both models demonstrate broadly comparable response patterns, indicating a modest degree of subject dependency in their classification behavior. A more detailed analysis of variability across subjects reveals that differences in classification performance may be attributed to several factors, including signal quality and inter-subject heterogeneity. Variations in EEG signal quality, such as residual artifacts, noise contamination, and differences in recording conditions, can influence the stability of extracted connectivity features. In addition, inter-subject heterogeneity in neural dynamics, including differences in AUD severity, duration of alcohol exposure, and individual brain network organization, may contribute to inconsistencies in classification outcomes. These factors are particularly relevant in EEG-based studies, where both physiological variability and acquisition-related noise can significantly impact model generalization [14, 36]. The observed variability highlights the importance of developing more robust feature representations and incorporating subject-independent validation strategies to improve the reliability of EEG-based AUD classification.

The Ensemble model consistently delivers more favorable outcomes across precision, specificity, and class-wise accuracy. These characteristics position it as a more reliable tool for AUD classification, meriting further exploration and validation in larger, more diverse datasets to assess its potential for deployment in real-world clinical environments.

3.6 Performance comparison with related work

Table 7 presents a comparison of the proposed approach with representative studies in EEG- and neuroimaging-based classification. It should be noted that direct numerical comparison across studies is inherently limited due to differences in datasets, experimental protocols, feature extraction methods, and evaluation settings. The studies included in this table vary in terms of data modality (EEG vs. fMRI), task conditions (resting-state vs. task-based), sample size, and validation strategies, which may influence reported performance metrics.

Accordingly, the purpose of this comparison is not to establish a strict benchmark, but rather to provide contextual insight into how the proposed method relates to existing approaches in the literature. In particular, the table highlights the diversity of methodologies employed, including time–frequency analysis, deep learning architectures, and connectivity-based techniques.

Within this broader context, the proposed fractal-informed FC approach demonstrates competitive performance while maintaining a relatively simple and interpretable signal-processing pipeline. Unlike more complex deep learning models, the present method focuses on feature representation by separating oscillatory and scale-free components prior to connectivity estimation, enabling a more structured analysis of EEG signal characteristics.

Nevertheless, a more rigorous evaluation would require implementing standard FC pipelines and alternative feature extraction methods on the same dataset for direct comparison. Such a controlled benchmarking study is beyond the scope of the current work but represents an important direction for future research to further validate the effectiveness of the proposed approach.

4. CONCLUSION

This study presents a signal-processing–oriented framework for the characterization of AUD using EEG-derived FC features informed by fractal decomposition. By separating oscillatory and scale-free components prior to connectivity estimation, the proposed approach enables a more detailed examination of neural interactions that extend beyond conventional frequency-domain representations.

The results demonstrate that fractal-based FC features capture meaningful network-level signal characteristics associated with AUD-related neural alterations. Comparative analyses of original, fractal, and non-fractal connectivity components reveal that, while original connectivity features retain strong discriminative information, the non-fractal and fractal components contribute complementary insights by emphasizing scale-invariant and background signal behavior. These findings underscore the value of fractal-informed representations in enhancing the interpretability and robustness of EEG-based connectivity analysis.

Signal decomposition plays a pivotal role in enhancing the interpretability and robustness of EEG connectivity analysis. Classification results obtained using the Optimizable SVM and Ensemble Learning models confirm the effectiveness of the extracted features, with the Ensemble classifier achieving the highest overall performance. Importantly, the role of machine learning in this work is confined to validation, reinforcing that the observed performance gains arise primarily from the underlying signal representation rather than from classifier complexity.

Overall, the proposed fractal-based connectivity framework advances biomedical signal processing for EEG analysis by

integrating scale-free signal modeling with network-level interpretation. The approach shows strong potential as a foundation for objective and non-invasive assessment of neurological disorders. Future work will focus on validating the framework using larger and more diverse datasets, as well as exploring alternative connectivity measures and decomposition strategies to further enhance signal characterization and generalizability.

ACKNOWLEDGMENT

This work was supported by Yayasan Universiti Teknologi PETRONAS under Grant number YUTP-FRG 015LC0-539.

The authors would like to thank the HiCOE Centre for Intelligent Signal and Imaging Research (CISIR), Universiti Teknologi PETRONAS, for providing the necessary facilities and support to carry out this research.

REFERENCES

[1] IARC Working Group on the Evaluation of Carcinogenic Risks to Humans. (1988). Alcohol Drinking. Vol. 44. IARC Monographs, Lyon, France. https://www.ncbi.nlm.nih.gov/books/NBK531662/.

[2] Miller, A.P., Kuo, S.I., Johnson, E.C., Tillman, R., et al. (2023). Diagnostic criteria for identifying individuals at high risk of progression from mild or moderate to severe Alcohol Use Disorder. JAMA Network Open, 6(10): e2337192. https://doi.org/10.1001/jamanetworkopen.2023.37192

[3] Oscar-Berman, M., Marinković, K. (2007). Alcohol: Effects on neurobehavioral functions and the brain. Neuropsychology Review, 17: 239-257. https://doi.org/10.1007/s11065-007-9038-6

[4] Valenzuela, C.F. (1997). Alcohol and neurotransmitter interactions. Alcohol Health and Research World, 21(2): 144-148. https://pmc.ncbi.nlm.nih.gov/articles/PMC6826822/.

[5] Chikritzhs, T., Livingston, M. (2021). Alcohol and the risk of injury. Nutrients, 13(8): 2777. https://doi.org/10.3390/nu13082777

[6] Egervari, G., Siciliano, C.A., Whiteley, E.L., Ron, D. (2021). Alcohol and the brain: From genes to circuits. Trends in Neurosciences, 44(12): 1004-1015. https://doi.org/10.1016/j.tins.2021.09.006

[7] Raichle, M.E., MacLeod, A.M., Snyder, A.Z., Powers, W.J., Gusnard, D.A., Shulman, G.L. (2001). A default mode of brain function. Proceedings of the National Academy of Sciences, 98(2): 676-682. https://doi.org/10.1073/pnas.98.2.676

[8] American Psychiatric Association. (2013). Diagnostic and Statistical Manual of Mental Disorders, Fifth Edition. Arlington, USA. https://doi.org/10.1176/appi.books.9780890425596

[9] Kamarajan, C., Ardekani, B.A., Pandey, A.K., Chorlian, D.B., et al. (2020). Random forest classification of Alcohol Use Disorder using EEG source functional connectivity, neuropsychological functioning, and impulsivity measures. Behavioral Sciences, 10(3): 62. https://doi.org/10.3390/bs10030062

[10] Sión, A. Bruña Fernández, R., Martínez Maldonado, A., Domínguez Centeno, I., Torrado-Carvajal, A., Rubio, G., Pereda, E., Jurado-Barba, R. (2020). Resting-state connectivity and network parameter analysis in alcohol-dependent males. A simultaneous EEG-MEG study. Journal of Neuroscience Research, 98(10): 1857-1876. https://doi.org/10.1002/jnr.24673

[11] Ehlers, C.L., Havstad, J.W., Schuckit, M.A. (1995). EEG dimension in sons of alcoholics. Alcoholism: Clinical and Experimental Research, 19(4): 992-998. https://doi.org/10.1111/j.1530-0277.1995.tb00979.x

[12] Suk, J.W., Hwang, S., Cheong, C. (2021). Functional and structural alteration of default mode, executive control, and salience networks in Alcohol Use Disorder. Frontiers in Psychiatry, 12: 742228. https://doi.org/10.3389/fpsyt.2021.742228

[13] Dorvashi, M., Behzadfar, N., Shahgholian, G. (2023). An efficient method for classification of alcoholic and normal electroencephalogram signals based on selection of an appropriate feature. Journal of Medical Signals & Sensors, 13(1): 11-20. https://doi.org/10.4103/jmss.jmss_183_21

[14] Kutluana, G., Türker, İ. (2024). Classification of cardiac disorders using weighted visibility graph features from ECG signals. Biomedical Signal Processing and Control, 87: 105420. https://doi.org/10.1016/j.bspc.2023.105420

[15] Miljevic, A., Bailey, N.W., Murphy, O.W., Perera, M.P.N., Fitzgerald, P.B. (2023). Alterations in EEG functional connectivity in individuals with depression: A systematic review. Journal of Affective Disorders, 328: 287-302. https://doi.org/10.1016/j.jad.2023.01.126

[16] Chaki, J., Woźniak, M. (2023). A deep learning based four-fold approach to classify brain MRI: BTSCNet. Biomedical Signal Processing and Control, 85: 104902. https://doi.org/10.1016/j.bspc.2023.104902

[17] Shen, M., Wen, P., Song, B., Li, Y. (2023). Automatic identification of schizophrenia based on EEG signals using dynamic functional connectivity analysis and 3D convolutional neural network. Computers in Biology and Medicine, 160: 107022. https://doi.org/10.1016/j.compbiomed.2023.107022

[18] Xu, M., Zhang, Y., Zhang, Y., Liu, X., Qing, K. (2024). EEG biomarkers analysis in different cognitive impairment after stroke: An exploration study. Frontiers in Neurology, 15: 1358167. https://doi.org/10.3389/fneur.2024.1358167

[19] Shen, M.K., Wen, P., Song, B., Li, Y. (2023). Detection of alcoholic EEG signals based on whole brain connectivity and convolution neural networks. Biomedical Signal Processing and Control, 79: 104242. https://doi.org/10.1016/j.bspc.2022.104242

[20] Chenniappan, R., Viswanathan, C., Duraisamy, V.A. (2025). EEGNet: Detection and diagnosis of EEG signals for Epilepsy disease using weighted empirical mode decomposition and EEGNet architecture. Traitement du Signal, 42(4): 2417-2430. https://doi.org/10.18280/ts.420448

[21] Wang, Y.T., Chen, Y., Cui, Y., Zhao, T., et al. (2024). Alterations in electroencephalographic functional connectivity in individuals with major depressive disorder: A resting-state electroencephalogram study. Frontiers in Neuroscience, 18: 1412591. https://doi.org/10.3389/fnins.2024.1412591

[22] Chang, Y., Wang, X.J., Liao, J.M., Chen, S.T., Liu, X.Y., Liu, S., Ming, D. (2024). Temporal hyper-connectivity and frontal hypo-connectivity within gamma band in

schizophrenia: A resting state EEG study. Schizophrenia Research, 264: 220-230. https://doi.org/10.1016/j.schres.2023.12.017
[23] Mohd Nazri, A.K. Yahya, N., Khan, D.M., Mohd Radzi, N.Z., Badruddin, N., Abdul Latiff, A.H., Abdulaal, M.J. (2025). Partial directed coherence analysis of resting-state EEG signals for Alcohol Use Disorder detection using machine learning. Frontiers in Neuroscience, 18: 1524513. https://doi.org/10.3389/fnins.2024.1524513
[24] Elsayed, M. Syan, S.K., Belisario, K.L., MacKillop, E., Amlung, M., Sweet, L.H., MacKillop, J. (2025). Resting-state functional connectivity and Alcohol Use Disorder: A case-control study. The Journal of Neuropsychiatry and Clinical Neurosciences, 38(2). https://doi.org/10.1176/appi.neuropsych.20240145
[25] Yang, L.J., Wei, X.G., Liu, F.R., Zhu, X.R., Zhou, F. (2023). Automatic feature learning model combining functional connectivity network and graph regularization for depression detection. Biomedical Signal Processing and Control, 82: 104520. https://doi.org/10.1016/j.bspc.2022.104520
[26] Xu, Y.J., Yu, Z.J., Li, Y.S., Liu, Y.H., Li, Y., Wang, Y.S. (2024). Autism spectrum disorder diagnosis with EEG signals using time series maps of brain functional connectivity and a combined CNN–LSTM model. Computer Methods and Programs in Biomedicine, 250: 108196. https://doi.org/10.1016/j.cmpb.2024.108196
[27] Li, H.C., Wu, L. (2022). EEG classification of normal and alcoholic by deep learning. Brain Sciences, 12(6): 778. https://doi.org/10.3390/brainsci12060778
[28] Khan, D.M., Yahya, N., Kamel, N., Faye, I. (2021). Effective connectivity in default mode network for alcoholism diagnosis. IEEE Transactions on Neural Systems and Rehabilitation Engineering, 29: 796-808. https://doi.org/10.1109/TNSRE.2021.3075737
[29] Buchanna, G. Premchand, P., Govardhan, A. (2022). Classification of epileptic and non-epileptic Electroencephalogram (EEG) signals using fractal analysis and support vector regression. Emerging Science Journal, 6(1): 138-144. https://doi.org/10.28991/ESJ-2022-06-01-011
[30] Erbil, N., Deshpande, G. (2025). Scale-free dynamics of resting-state fMRI microstates. Fractal and Fractional, 9(2): 112. https://doi.org/10.3390/fractalfract9020112
[31] Sadiq, A. Yahya, N., Tang, T.B., Hashim, H., Naseem, I. (2022). Wavelet-based fractal analysis of rs-fMRI for classification of Alzheimer's disease. Sensors, 22(9): 3102. https://doi.org/10.3390/s22093102
[32] Hadiyoso, S., Wijayanto, I., Humairani, A. (2023). Entropy and fractal analysis of EEG signals for early detection of Alzheimer's Dementia. Traitement du Signal, 40(4): 1673-1679. https://doi.org/10.18280/ts.400435
[33] Valentim, C.A., Inacio, C.M.C., David, S.A. (2021). Fractal methods and power spectral density as means to explore EEG patterns in patients undertaking mental tasks. Fractal and Fractional, 5(4): 225. https://doi.org/10.3390/fractalfract5040225
[34] Menon, V. (2023). 20 years of the default mode network: A review and synthesis. Neuron, 111(16): 2469-2484. https://doi.org/10.1016/j.neuron.2023.04.023
[35] Ye, C.Q., Li, J., Chen, X.B., Hou, Y.Y. (2023). A feasible semi-quantum private comparison based on entanglement swapping of Bell states. Physica A: Statistical Mechanics and its Applications, 625: 129023. https://doi.org/10.1016/j.physa.2023.129023
[36] Chen, C.L., Xu, S.Y., Zhou, J.X., Yi, C.L., Yu, L., Yao, D.Z., Zhang, Y.S., Li, F.L., Xu, P. (2025). Resting-state EEG network variability predicts individual working memory behavior. NeuroImage, 310: 121120. https://doi.org/10.1016/j.neuroimage.2025.121120
[37] Sandrone, S., Catani, M. (2013). Journal club: Default-mode network connectivity in cognitively unimpaired patients with Parkinson disease. Neurology, 81(23): e172-e175. https://doi.org/10.1212/01.wnl.0000436943.62904.09
[38] Choi, K.M. Kim, J.Y., Kim, Y.W., Han, J.W., Im, C.H., Lee, S.H. (2021). Comparative analysis of default mode networks in major psychiatric disorders using resting-state EEG. Scientific Reports, 11: 22007. https://doi.org/10.1038/s41598-021-00975-3
[39] Neuner, I., Arrubla, J., Werner, C.J., Hitz, K., Boers, F., Kawohl W., Shah, N.J. (2014). The default mode network and EEG regional spectral power: A simultaneous fMRI-EEG study. PLOS ONE, 9(2): e88214. https://doi.org/10.1371/journal.pone.0088214
[40] BRMLAB. (2020). Closest 10-10 Electrode position to each Brodmann area. https://brmlab.cz/project/brain_hacking/broadmannarea.
[41] Wang, S.L., Zhang, J.S., Shao, Z.H., Deng, H.D., Wang, C.J., Wang, J.L., Wang, C.S. (2025). Alcohol cue processing alters delta-band functional connectivity and theta-band network topology in Alcohol Use Disorder: A task-based EEG study. BMC Psychiatry, 25: 1206. https://doi.org/10.1186/s12888-025-07629-y
[42] Wen, H.G., Liu, Z.M. (2016). Separating fractal and oscillatory components in the power spectrum of neurophysiological signal. Brain Topography, 29: 13-26. https://doi.org/10.1007/s10548-015-0448-0
[43] You, W., Achard, S., Stadler, J., Brückner, B., Seiffert, U. (2012). Fractal analysis of resting state functional connectivity of the brain. In the 2012 International Joint Conference on Neural Networks (IJCNN), Brisbane, QLD, Australia, pp. 1-8. https://doi.org/10.1109/IJCNN.2012.6252657
[44] Sadiq, A., Al-Hiyali, M.I., Yahya, N., Tang, T.B., Khan, D.M. (2022). Non-oscillatory connectivity approach for classification of autism spectrum disorder subtypes using resting-state fMRI. IEEE Access, 10: 14049-14061. https://doi.org/10.1109/ACCESS.2022.3146719
[45] Norashikin (2026). Fractal decomposition, https://www.mathworks.com/matlabcentral/fileexchange/181799-fractal-decompositon, accessed on Apr. 12, 2026.
[46] Canessa, N., Basso, G., Manera, M., Poggi, P., Gianelli, C. (2023). Functional coherence in intrinsic frontal executive networks predicts cognitive impairments in Alcohol Use Disorder. Brain Sciences, 13(1): 45. https://doi.org/10.3390/brainsci13010045
[47] Song, Z.Y., Chen, J., Wen, Z., Zhang, L. (2020). Abnormal functional connectivity and effective connectivity between the default mode network and attention networks in patients with alcohol-use disorder. Acta Radiologica, 62(2): 251-259. https://doi.org/10.1177/0284185120923270
[48] Rice, L.C., Langan, M.T., Cheng, D.T., Sheu, Y.S., et al. (2023). Disrupted executive cerebro-cerebellar functional connectivity in Alcohol Use Disorder.

Alcohol, Clinical and Experimental Research, 48(1): 33-47. https://doi.org/10.1111/acer.15219

[49] Crespi, C., Galandra, C., Canessa, N., Manera, M., Poggi, P., Basso, G. (2020). Microstructural damage of white-matter tracts connecting large-scale networks is related to impaired executive profile in Alcohol Use Disorder. NeuroImage: Clinical, 25: 102141. https://doi.org/10.1016/j.nicl.2019.102141

[50] Guerrero, D., Dzemidzic, M., Moghaddam, M., Liu, M.T., et al. (2025). Resting state functional connectivity patterns associate with Alcohol Use Disorder characteristics: Insights from the triple network model. NeuroImage: Clinical, 49: 103939. https://doi.org/10.1016/j.nicl.2025.103939